arXiv:1601.01485v2 [physics.plasm-ph] 21 Apr 2016

# Sensitivity of alpha-particle–driven Alfvén eigenmodes to q-profile variation in ITER scenarios

**P. Rodrigues[1], A. C. A. Figueiredo[1], D. Borba[1], R. Coelho[1], L. Fazendeiro[1], J. Ferreira[1], N. F. Loureiro[1,2], F. Nabais[1], S. D. Pinches[3], A. R. Polevoi[3], and S. E. Sharapov[4]**

[1]Instituto de Plasmas e Fusão Nuclear, Instituto Superior Técnico, Universidade de Lisboa, 1049-001 Lisboa, Portugal.
[2]Plasma Science and Fusion Center, Massachusetts Institute of Technology, Cambridge, MA 02139, USA.
[3]ITER Organization, Route de Vinon-sur-Verdon, 13067 St Paul-lez-Durance Cedex, France.
[4]CCFE, Culham Science Centre, Abingdon OX14 3DB, United Kingdom.

E-mail: par@ipfn.ist.utl.pt

**Abstract.** A perturbative hybrid ideal-MHD/drift-kinetic approach to assess the stability of alpha-particle–driven Alfvén eigenmodes in burning plasmas is used to show that certain foreseen ITER scenarios, namely the $I_\mathrm{p} = 15$ MA baseline scenario with very low and broad core magnetic shear, are sensitive to small changes in the background magnetic equilibrium. Slight variations (of the order of 1%) of the safety-factor value on axis are seen to cause large changes in the growth rate, toroidal mode number, and radial location of the most unstable eigenmodes found. The observed sensitivity is shown to proceed from the very low magnetic shear values attained throughout the plasma core, raising issues about reliable predictions of alpha-particle transport in burning plasmas.

PACS numbers: 28.52.Av, 52.35.Bj, 52.55.Pi

## 1. Introduction

Plasma heating during the burning regime in tokamak reactors will rely upon the energy of fusion-born alpha-particles, which must be kept confined to ensure efficient heating and that power fluxes remain within the design values of the ITER plasma facing components [1]. However, such particles can drive Alfvén Eigenmodes (AEs) unstable and be thus transported away from the plasma core, which would hamper the burning process [2,3]. In order to predict the level of alpha-particle redistribution and loss that is expected for a given fusion scenario, the most unstable AEs need to be identified first so that their stability properties can be employed in further analysis.

Understanding the complex interplay between energetic suprathermal particles and AEs is a key step in the fusion research effort [2–4], particularly in preparation for future burning-plasma experiments. Recent research concerning ITER [5–8] has been focusing on the 15 MA baseline scenario, with on-axis safety factor close to unity and low magnetic shear throughout the plasma core [9]. Low magnetic-shear profiles are indeed expected to take place during planned ITER operation due to sawtooth activity, which periodically redistributes the toroidal current density within a large mixing region that may extend to about half of the plasma minor radius because safety-factor values at the boundary are low ($q_\mathrm{b} \sim 3$) [10,11]. In addition, low magnetic shear was found to play a significant role in the nonlinear stabilization of microturbulence by suprathermal pressure gradients [12] — an important observation especially in cases where sheared toroidal momentum is insufficient to provide the said stabilization [13,14].

In this work, a perturbative hybrid ideal-MHD/drift-kinetic plasma model is used to find how the stability properties of AEs change in response to small variations of the background magnetic equilibrium. Of particular interest are the net growth rate, wave number, and frequency of the most unstable AEs. These properties are shown to be significantly affected by small changes of the safety-factor profile, which are achieved through slight variations of the total plasma current. Such high sensitivity is also shown to be caused by the low levels of magnetic shear present in the scenario under analysis.

## 2. Particle-wave interaction model

Routine stability assessments in burning plasmas can be accomplished with an hybrid MHD–drift-kinetic model of particle-wave interaction [7]. Here, ideal-MHD theory is used to describe thermal species (DT fuel ions, electrons, He ash and other impurities), whose energy distribution functions are assumed to be local Maxwellians. The radial dependence of their temperature and particle-number density is an input to the model. A similar input must also be provided for the density of the suprathermal, diluted, fusion-born alpha-particle population, which is assumed to be isotropic in pitch angle. Its energy distribution function is described by the model [15]

$$f_\mathrm{sd}(E) = \frac{C_\mathrm{N}}{E^{3/2} + E_\mathrm{c}^{3/2}} \operatorname{erfc}\big[(E - E_0)/\Delta_\mathrm{E}\big], \tag{1}$$

where $C_\mathrm{N}$ is a normalization constant while $E_\mathrm{c}$, $\Delta_\mathrm{E}$, and $E_0$ are radius-independent parameters, and erfc is the complementary error function.

The response of the non-Maxwellian alpha-particle population to an ideal-MHD perturbation of the thermal plasma is found solving the linearized drift-kinetic

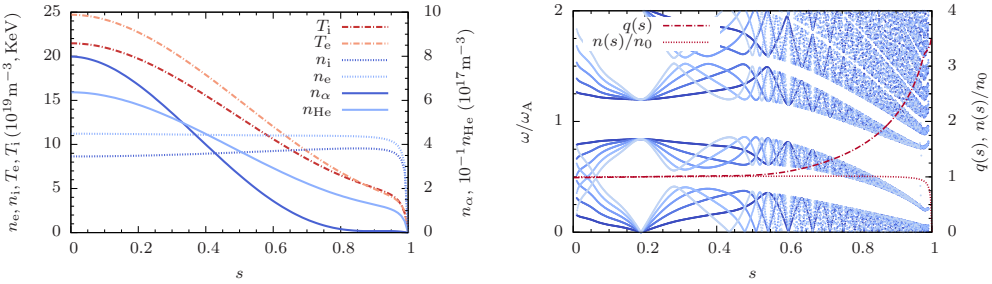


**Figure 1.** Radial distribution of the plasma-species densities and temperatures (left). Ideal Alfvén continua for toroidal mode numbers $n = 10, \ldots, 50$ (from dark to light hues), safety factor, and normalized mass density (right).

equation [16], valid in the limit

$$\omega/\Omega_\alpha \sim \left(k_\perp \rho_\alpha\right)^2 \ll 1, \tag{2}$$

with $\omega$ and $k_\perp$ the AE frequency and perpendicular wave number, whereas $\Omega_\alpha$ and $\rho_\alpha$ are the alpha-particle gyro-frequency and gyro-radius. This response gives rise to a small complex correction $\delta\omega$ to the frequency $\omega$ of marginally stable AEs and the alpha-particle contribution to their growth rate is then $\gamma_\alpha = \mathrm{Im}(\delta\omega)$. A similar procedure for each thermal species $j$ produces the corresponding Landau-damping contribution $\gamma_j$ to the wave-particle energy exchange. Disregarding effects not contained in the ideal-MHD framework (e.g., Alfvén-continuum damping, radiative damping), which cannot be modeled by the perturbative approach just described, the overall AE growth rate is thus $\gamma_\alpha + \sum_j \gamma_j$.

The workflow to assess the stability of a given plasma configuration is as follows [7]: a magnetic equilibrium is first computed with `HELENA` [17], using pressure and current-density profiles obtained from transport modelling, and then all possible AEs are found by intensively scanning over a frequency and wave-number range with the ideal-MHD code `MISHKA` [18], while the energy transfer between them and all plasma species is evaluated with the drift-kinetic code `CASTOR-K` [19, 20]. The computational efficiency of the `MISHKA`/`CASTOR-K` pair is the key to handle the very large number of AEs involved in such systematic stability assessments.

## 3. The reference case

The radial distribution of each species' particle-density and temperature for the ITER $I_\mathrm{p} = 15$ MA baseline scenario [9] were found with the transport code `ASTRA` [21] and are displayed in figure 1, where $s^2 = \psi/\psi_\mathrm{b}$, $\psi$ is the poloidal flux, and $\psi_\mathrm{b}$ is its value at the boundary. Other relevant parameters are the on-axis magnetic field $B_0 = 5.3$ T, the minor radius $a = 2$ m, and the magnetic-axis location at $R_0 = 6.4$ m (not to be confused with the tokamak's geometric axis $R_\mathrm{vac} = 6.2$ m). The DT fuel mix ratio is $n_\mathrm{D}/n_\mathrm{T} = 1$ and their combined density is $n_\mathrm{i} = n_\mathrm{D} + n_\mathrm{T}$. Peaked temperature profiles contrast with DT-ion and electron density distributions, which are flat almost up to the plasma edge. In turn, fusion alpha-particles are mostly concentrated in the core, with an almost constant gradient $\mathrm{d}n_\alpha/\mathrm{d}s$ for $0.3 \lesssim s \lesssim 0.5$.

Flat mass-density distributions up to the plasma edge, like the one plotted in figure 1, contribute to the closing of the frequency gaps in the Alfvén continuum

arising from the coupling between distinct poloidal harmonics. Consequently, AEs with frequencies in such gaps can hardly extend towards the plasma boundary without interacting with the Alfvén continuum and thus undergo significant damping. This property acts as a filter regarding the type of AEs that can be found for the particular plasma state being considered. Actually, the safety-factor profile also depicted in figure 1 (right panel) is almost flat in the core region ($s \lesssim 0.5$), yielding well separated gaps for toroidal mode numbers $n \gtrsim 10$. Highly localized low-shear toroidicity-induced AEs (LSTAEs), with only two dominant poloidal harmonics, are therefore expected to arise in the core. Conversely, on the outer half of the plasma the magnetic shear is higher, radial gap separation is smaller, and AEs become broader, encompassing a large number of poloidal harmonics and extending to the edge. In so doing, they interact with the Alfvén continuum and are thus excluded from further analysis, which will be dominated by $n \gtrsim 10$ highly localized LSTAEs.

Contrary to the safety-factor profile, which establishes each AE location, the square root of the density profile influences only the value of the Alfvén velocity. Therefore, no significant sensitivity is expected to small changes in $n_\mathrm{i}$ or $n_\mathrm{e}$. On the other hand, and for the same value on-axis, density distributions less flat than that in figure 1 have lower density near the edge, which contributes to raise the local continuum frequency and therefore allow broader AEs to extend up to the edge. Without significant interaction with the Alfvén continuum, these broader AEs could influence the overall stability properties of the considered scenario. A detailed study of the consequences of such density-profile shaping is, however, beyond the scope of this work.

The $(\omega, \mathbf{k})$-space scan carried out by `MISHKA` finds the radial structure of all AEs with toroidal number $n$ in the range $1 \leqslant n \leqslant 50$ and poloidal harmonics $n - 1 \leqslant m \leqslant n + 15$. The limit of 17 poloidal harmonics is set by pragmatic considerations: more harmonics would benefit the convergence of broad-width AEs only, which would nonetheless undergo continuum damping at some radial location since their frequency gap is closed. In turn, the upper limit for $n$ is set by the drift-kinetic ordering in (2) as

$$k_\perp \rho_\alpha \lesssim 1, \quad \text{whence} \quad n \lesssim \big(s/q\big)\big/\big(\rho_\alpha/a\big) \approx 50, \tag{3}$$

with $\rho_\alpha/a \approx 10^{-2}$ the normalized alpha-particle gyro-radius, $k_\perp \sim \big(nq\big)\big/\big(as\big)$, $q \approx 1$, and $s \approx 0.5$. For each $n$, the frequency range $0 \leqslant \omega/\omega_\mathrm{A} \leqslant 1$ [where $\omega_\mathrm{A} = V_\mathrm{A}/R_0$, with $V_\mathrm{A}$ the on-axis Alfvén velocity] is sampled in small steps of size $2 \times 10^{-5}$. Next, `CASTOR-K` evaluates the energy exchange between every AE found and each of the plasma species considered, yielding the corresponding growth (or damping) rate. The parameters of the energy distribution-function model in (1) for the fusion-born alpha particles were taken at a radial location ($s \approx 0.4$) near the maximum gradient of their density profile, yielding the values $E_\mathrm{c} = 730$ KeV, $\Delta_\mathrm{E} = 50$ KeV, and $E_0 = 3.5$ MeV.

The stability assessment is summarized in figure 2 (left panel) for the reference scenario where the plasma current $I_\mathrm{p}$ takes the reference value $I_\mathrm{ref} = 15$ MA and the on-axis safety factor is $q_\mathrm{ref} = 0.987$. This is essentially a subset of previous results [7], here restricted to toroidicity-induced AEs (TAEs) to make the presentation of results clearer (whence the upper limit $\omega/\omega_\mathrm{A} \leqslant 1$ set on the AEs' frequency). The most unstable TAEs found have $20 \lesssim n \lesssim 30$ and lie in the core ($0.3 \lesssim s_\mathrm{max} \lesssim 0.5$, with $s_\mathrm{max}$ the location of their maximum amplitude), where $\mathrm{d}n_\alpha/\mathrm{d}s$ is highest and the magnetic shear is lowest. Conversely, AEs located in the outer half of the plasma ($0.5 \lesssim s_\mathrm{max} \lesssim 0.8$) are mostly stable due to smaller values of the alpha-particle density

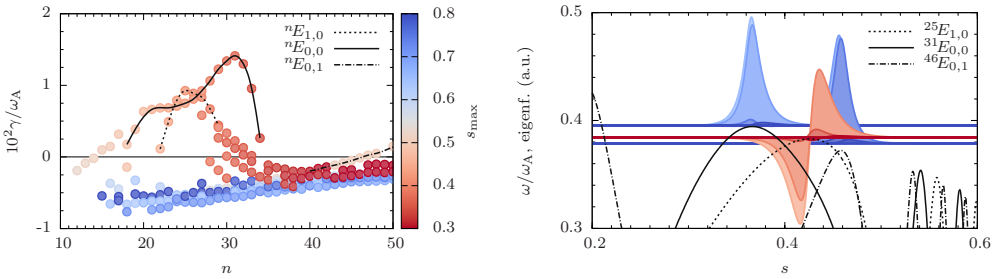


**Figure 2.** Distribution of the normalized growth rate $\gamma/\omega_A$ by $n$ for $I_{ref}$, with each TAE colored by the radial location of its maximum amplitude, and three TAE families identified by dotted, solid, and dash-dotted lines (left). Example eigenfunctions of the AE families $^nE_{0,1}$, $^nE_{1,0}$, and $^nE_{0,0}$ (right), with baselines at their normalized frequencies (filled curves) and their corresponding ideal Alfvén continua (solid, dotted, and dash-dotted lines).

$n_\alpha$ and its gradient $\mathrm{d}n_\alpha/\mathrm{d}s$.

Three lines are plotted in figure 2 (left) connecting TAEs belonging to three families that will play a key role in the ensuing discussion. These families are denoted as $^nE_{l,p}$, meaning that their members are LSTAEs with even ($E$) parity and $l$ zeros, with $p$ being the difference between the first dominant poloidal harmonic and the toroidal number $n$. A member of each family has its radial structure depicted in the right panel of figure 2, where they can be identified by their respective Alfvén continua.

## 4. Small changes in magnetic equilibria

The reference value $I_{ref} = 15$ MA considered in the stability analysis that led to figure 2 is only nominal. In practice, ITER operation under this baseline scenario will exhibit values of the plasma current which are close, but of course not rigorously equal to, the reference $I_{ref}$. Therefore, details of the safety-factor profile near the magnetic axis are not accurately established and can, eventually, change the stability properties of the AEs found. Other factors that may cause a similar impact include the presence of pressure anisotropy concurrently with low magnetic-shear configurations [22].

To explore the dependence of AE stability properties on safety-factor uncertainty, two different magnetic equilibria are next considered, in addition to the reference one discussed in the previous Section. These equilibria are obtained by changing $I_p$ from $I_{ref}$ by the small amounts $-\delta$ and $\delta/2$, with $\delta = 0.16$ MA, whilst keeping the same equilibrium profiles $p'(\psi)$ and $f(\psi)f'(\psi)$. The resulting safety-factor profiles are plotted in figure 3 (left) with the reference one for comparison. As expected, the on-axis safety factor value $q_0$ changes only slightly by circa 1% and 0.5% respectively, thus following the magnitude of $I_p$ variations away from $I_{ref}$. Moreover, the safety-factor slope in the plasma core is kept almost unchanged in the two cases, with $q_0' \approx 0.07$.

The consequences to the stability properties are displayed in figure 3 (right), where small variations ($\sim 1\%$) in $I_p$ or $q_0$ are seen to cause large changes in the toroidal number ($\sim 20\%$) and normalized growth rate ($\sim 50\%$) of the most unstable AEs. Raising $q_0$ (and thus decreasing $I_p$) pushes the most unstable AE families ($^nE_{0,0}$ and $^nE_{1,0}$) towards lower $n$ and up to larger growth rates. A slight decrease in $q_0$ yields the opposite. In both cases, the most unstable AEs are still even LSTAEs.

This extreme sensitivity to small changes in the background magnetic equilibrium

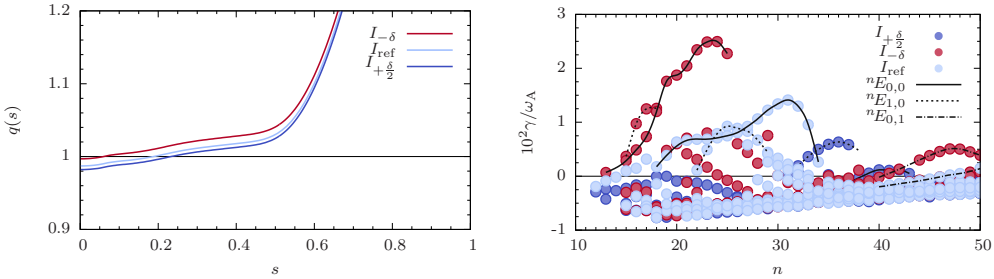


**Figure 3.** Left: Safety-factor profiles for the reference plasma current and two slightly different $I_{\rm p}$ values. Right: Distribution of the normalized growth rate $\gamma/\omega_{\rm A}$ by $n$ for the three plasma-current values, with indication of the three TAE families.

can be understood with the aid of the three conditions:

$$q \simeq q_0 + q_0' s, \tag{4}$$

$$q = 1 + \frac{1}{2n}, \tag{5}$$

and

$$k_\perp \Delta_{\rm orb} \simeq \left(\frac{nq}{as}\right)\left(\frac{aq}{\varepsilon\tilde{\Omega}}\right) \sim 1. \tag{6}$$

The first one is a linear representation of the safety factor profile in the low-shear core and the second defines the resonant surface of each TAE in the ${}^nE_{l,0}$ families. In turn, the third relation is a condition for efficient drive, with $\Delta_{\rm orb} \sim (aq)/(\epsilon\tilde{\Omega})$ the orbit width of an alpha-particle travelling at the Alfvén velocity with a very small pitch angle, $\tilde{\Omega} = \Omega_\alpha/\omega_{\rm A}$ its normalized gyro-frequency, and $\varepsilon = a/R_0$ the equilibrium inverse aspect ratio. Together, these three equations set the three variables $n$, $q$, and $s$ (respectively, toroidal mode number, safety factor, and radial location) corresponding to the most unstable AEs in terms of the four parameters $q_0$, $q_0'$, $\varepsilon$, and $\tilde{\Omega}$. Eliminating $s$ and $q$ from equations (4), (5), and (6), one finds the toroidal number to follow the relation

$$n + \frac{1-2\zeta}{4n} + 1 = \zeta(1-q_0), \tag{7}$$

which is written in terms of the dimensionless number

$$\zeta \equiv \frac{\varepsilon\tilde{\Omega}}{q_0'} = \left(\frac{q}{q_0'}\right)\Big/\left(\frac{\Delta_{\rm orb}}{a}\right). \tag{8}$$

Subtracting from equation (7) its evaluation with the values $n_{\rm ref}$ and $q_{\rm ref}$ corresponding to the reference case, gives

$$\left(1 + \frac{2\zeta - 1}{4n_{\rm ref}\, n}\right)(n - n_{\rm ref}) = -\zeta(q_0 - q_{\rm ref}), \tag{9}$$

which relates a variation of the on-axis safety factor with a corresponding change in the toroidal number of the most unstable LSTAEs.

For the ITER scenario under consideration, parameters are $q_0' \approx 0.07$, $\varepsilon \approx 0.3$, and $\tilde{\Omega} \approx 230$, whence $\zeta \approx 10^3$. On the other hand, $n \sim n_{\rm ref} \sim 30$ and therefore $(2\zeta - 1)/(4n_{\rm ref} n) \sim 1/2$. Because the prefactor in the left-hand side of equation (9)

is of the order of unity, it is the large value attained by $\zeta$ in the right-hand side that forces small changes of the on-axis safety factor to cause large variations $n - n_{\mathrm{ref}}$. Also, one easily checks that increasing $q_0$ above $q_{\mathrm{ref}}$ lowers $n$ below $n_{\mathrm{ref}}$ and conversely, as observed in figure 3. Moreover, the conditions in equations (4), (5), and (6) relate the radial location $s$ of the most unstable AE with its toroidal number as

$$\varepsilon\tilde{\Omega}s = n\left(1 + \frac{1}{2n}\right)^2, \tag{10}$$

which predicts its displacement towards the core as $q_0$ increases and $n$ drops according to equation (9). As this happens, the AE growth rate rises due to the larger number of alpha-particles found as it moves inwards within the small region $0.3 \lesssim s \lesssim 0.4$, where $\mathrm{d}n_\alpha/\mathrm{d}s$ is negative and almost constant (figure 1). The consequences of decreasing $q_0$ (or raising $I_{\mathrm{p}}$) are likewise explained.

The contribution of the alpha-particle population to the AEs growth rate is [16]

$$\gamma_\alpha \propto \omega\frac{\partial f_\alpha}{\partial E} - n\frac{\partial f_\alpha}{\partial P_\phi}, \tag{11}$$

where $f_\alpha(E, P_\phi)$ is the unperturbed distribution function and

$$P_\phi = \frac{\psi_{\mathrm{b}}}{B_0 R_0^2}s^2 + \frac{1}{\tilde{\Omega}}\frac{RB_{(\phi)}}{R_0 B}\frac{v_\parallel}{V_{\mathrm{A}}} \tag{12}$$

is the normalized toroidal canonical momentum of a particle moving with velocity $v_\parallel$ parallel to a magnetic field with toroidal component $B_{(\phi)}$ and magnitude $B$. Because the derivative of (1) with respect to $E$ is always negative, alpha-particle drive results from the $P_\phi$ gradient. Such gradient relates with the radial derivative as

$$\frac{2\psi_{\mathrm{b}}}{B_0 R_0^2}\frac{\partial f_\alpha}{\partial P_\phi} \approx \frac{1}{s}\frac{\partial f_\alpha}{\partial s}, \tag{13}$$

if the location $s$ is not so close to the magnetic axis so that terms of order $(v_\parallel/V_{\mathrm{A}})/(\varepsilon\tilde{\Omega})$ can be neglected. Replacing equations (6) and (13) in (11) and discarding the energy-gradient term, the AEs radial location cancels out and one obtains

$$\gamma_\alpha \propto -\frac{\varepsilon\tilde{\Omega}}{q^2}\frac{\partial f_\alpha}{\partial s}. \tag{14}$$

Therefore, it may be asked if pushing unstable AEs further into the core, and consequently out of the region where the gradient $\mathrm{d}n_\alpha/\mathrm{d}s$ is strongest, may reduce $\gamma_\alpha$ and thus result in their stabilization. Such inward push is achieved by slightly increasing $q_0$ (hence reducing $I_{\mathrm{p}}$), which forces $n$ in equation (9) and $s$ in equation (10) to drop their values.

To address this question, two additional magnetic equilibria are considered with plasma currents $I_{-2\delta}$ and $I_{-5\delta}$ corresponding, respectively, to reductions of size $2\delta$ and $5\delta$ of the reference value $I_{\mathrm{ref}}$. Their safety-factor profiles are plotted in figure 4 (left) and $q_0$ now increases by 2% and 5% with respect to $q_{\mathrm{ref}}$. As a consequence, the surface $q = 1$ is removed from the plasma and solutions of the AE families ${}^nE_{l,0}$ can exist only if $n < \frac{1}{2}(q_0 - 1)^{-1}$.

The new stability assessment is summarized in figure 4 (right panel). According to predictions, AE families ${}^nE_{l,0}$ are pushed to lower $n$ and eventually vanish. For $I_{-2\delta}$ and before vanishing, AEs in the family ${}^nE_{0,0}$ have their growth rate reduced by 30% when compared to the reference case. The growth-rate reduction with respect to the case $I_{-\delta}$ is even larger. However, the AE family ${}^nE_{0,1}$ whose resonant surfaces

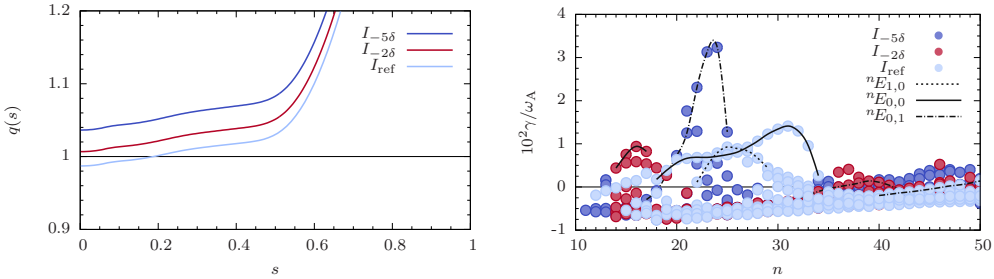


**Figure 4.** Safety-factor profiles for the reference plasma current and two other $I_{\rm p}$ values (left). Distribution of the normalized growth rate $\gamma/\omega_{\rm A}$ by $n$ for the three plasma-current values, with indication of the three TAE families.

are located at $q = 1 + \frac{3}{2n}$ is also brought to lower $n$ and inwards from its reference radial location. For $I_{-5\delta}$ these AEs are located near the maximum gradient $\mathrm{d}n_\alpha/\mathrm{d}s$ and their normalized growth rate peaks, accordingly, at 3.2% for $n = 24$. In this way, efforts to stabilize AEs by moving them out of the strong density-gradient region are thwarted by the destabilization of AE families previously stable or weakly unstable.

## 5. Conclusions

In summary, a perturbative hybrid ideal-MHD/drift-kinetic model was used to show that the stability properties of ITER $I_{\rm p} = 15$ MA baseline scenario are significantly sensitive to small changes of the safety-factor value on axis. Such small variations were shown to cause large changes in the growth rate, toroidal number, and radial location of the most unstable AEs. This sensitivity is not an artificial feature of the ideal-MHD/drift-kinetic model employed to describe the interaction between plasma species and AEs. On the contrary, it was shown to proceed from the large value attained by the dimensionless parameter $\zeta$, which is caused by the combination of large alpha-particle gyro-frequency [in equation (6)] with very low magnetic shear [in equation (4)] throughout a substantial domain within the plasma core.

If the large sensitivity of low magnetic-shear plasma configurations found in this work is still present in nonlinear analysis, then detailed simulations (e.g., suprathermal particle transport and redistribution by nonlinear interaction with AEs) carried out in such circumstances should take this fact into account, allowing a reasonable range of inputs in order to capture eventual large changes in their results. Moreover, strong operational consequences should also be expected, as such sensitivity would imply that AE instability and the alpha-particle radial transport it entails are, in fact, unpredictable given the extreme accuracy with which details about the safety factor profile would have to be known near the magnetic axis.

## Acknowledgments

This work was carried out within the framework of the EUROfusion Consortium and received funding from the Euratom research and training programme 2014-2018 under grant agreement no. 633053. IST activities received financial support from "Fundação para a Ciência e Tecnologia" (FCT) through project UID/FIS/50010/2013. ITER is the Nuclear Facility INB no. 174. The views and opinions expressed

herein do not necessarily reflect those of the European Commission, IST, CCFE, or the ITER Organization. All computations were carried out using the HELIOS supercomputer system at the Computational Simulation Centre of the International Fusion Energy Research Centre (IFERC-CSC) in Aomori, Japan, under the Broader Approach collaboration between Euratom and Japan implemented by Fusion for Energy and JAEA. PR was supported by EUROfusion Consortium grant no. WP14-FRF-IST/Rodrigues and NFL was supported by FCT grant no. IF/00530/2013.

## References

[1] Fasoli A, Gormenzano C, Berk H, Breizman B, Briguglio S, Darrow D, Gorelenkov N, Heidbrink W, Jaun A, Konovalov S, Nazikian R, Noterdaeme J M, Sharapov S, Shinohara K, Testa D, Tobita K, Todo Y, Vlad G and Zonca F 2007 *Nucl. Fusion* **47** S264
[2] Breizman B N and Sharapov S E 2011 *Plasma Phys. Control. Fusion* **53** 054001
[3] Gorelenkov N, Pinches S and Toi K 2014 *Nucl. Fusion* **54** 125001
[4] Sharapov S, Alper B, Berk H, Borba D, Breizman B, Challis C, Classen I, Edlund E, Eriksson J, Fasoli A, Fredrickson E, Fu G, Garcia-Munoz M, Gassner T, Ghantous K, Goloborodko V, Gorelenkov N, Gryaznevich M, Hacquin S, Heidbrink W, Hellesen C, Kiptily V, Kramer G, Lauber P, Lilley M, Lisak M, Nabais F, Nazikian R, Nyqvist R, Osakabe M, von Thun C P, Pinches S, Podesta M, Porkolab M, Shinohara K, Schoepf K, Todo Y, Toi K, Zeeland M V, Voitsekhovich I, White R, Yavorskij V, TG I E and Contributors J E 2013 *Nucl. Fusion* **53** 104022
[5] Pinches S D, Chapman I T, Lauber P W, Oliver H J C, Sharapov S E, Shinohara K and Tani K 2015 *Phys. Plasmas* **22** 021807
[6] Lauber P 2015 *Plasma Phys. Control. Fusion* **57** 054011
[7] Rodrigues P, Figueiredo A, Ferreira J, Coelho R, Nabais F, Borba D, Loureiro N, Oliver H and Sharapov S 2015 *Nucl. Fusion* **55** 083003
[8] Figueiredo A C A, Rodrigues P, Borba D, Coelho R, Fazendeiro L, Ferreira J, Loureiro N F, Nabais F, Pinches S D, Polevoi A and Sharapov S E 2016 Comprehensive evaluation of the linear stability of Alfvén eigenmodes driven by alpha particles in an ITER baseline scenario *Nucl. Fusion* submitted (*Preprint* arXiv:1601.06621 [physics.plasm-ph])
[9] Polevoi A R, Medvedev S Y, Mukhovatov V S, Kukushkin A S, Murakami Y, Shimada M and Ivanov A A 2002 *J. Plasma Fusion Res. SERIES* **5** 82
[10] Porcelli F, Boucher D and Rosenbluth M N 1996 *Plasma Phys. Control. Fusion* **38** 2163
[11] Hender T, Wesley J, Bialek J, Bondeson A, Boozer A, Buttery R, Garofalo A, Goodman T, Granetz R, Gribov Y, Gruber O, Gryaznevich M, Giruzzi G, Günter S, Hayashi N, Helander P, Hegna C, Howell D, Humphreys D, Huysmans G, Hyatt A, Isayama A, Jardin S, Kawano Y, Kellman A, Kessel C, Koslowski H, Haye R L, Lazzaro E, Liu Y, Lukash V, Manickam J, Medvedev S, Mertens V, Mirnov S, Nakamura Y, Navratil G, Okabayashi M, Ozeki T, Paccagnella R, Pautasso G, Porcelli F, Pustovitov V, Riccardo V, Sato M, Sauter O, Schaffer M, Shimada M, Sonato P, Strait E, Sugihara M, Takechi M, Turnbull A, Westerhof E, Whyte D, Yoshino R, Zohm H, the ITPA MHD D and Group M C T 2007 *Nucl. Fusion* **47** S128
[12] Citrin J, Jenko F, Mantica P, Told D, Bourdelle C, Garcia J, Haverkort J W, Hogeweij G M D, Johnson T and Pueschel M J 2013 *Phys. Rev. Lett.* **111**(15) 155001
[13] Burrell K H 1997 *Phys. Plasmas* **4** 1499–1518
[14] Doyle E, Houlberg W, Kamada Y, Mukhovatov V, Osborne T, Polevoi A, Bateman G, Connor J, Cordey J, Fujita T, Garbet X, Hahm T, Horton L, Hubbard A, Imbeaux F, Jenko F, Kinsey J, Kishimoto Y, Li J, Luce T, Martin Y, Ossipenko M, Parail V, Peeters A, Rhodes T, Rice J, Roach C, Rozhansky V, Ryter F, Saibene G, Sartori R, Sips A, Snipes J, Sugihara M, Synakowski E, Takenaga H, Takizuka T, Thomsen K, Wade M, Wilson H, Group I T P T, Database I C, Group M T, Pedestal I and Group E T 2007 *Nucl. Fusion* **47** S18
[15] Pinches S, Appel L, Candy J, Sharapov S, Berk H, Borba D, Breizman B, Hender T, Hopcraft K, Huysmans G and Kerner W 1998 *Comp. Phys. Comm.* **111** 133 – 149
[16] Porcelli F, Stankiewicz R, Kerner W and Berk H L 1994 *Phys. Plasmas* **1** 470–480
[17] Huysmans G, Goedbloed J and Kerner W 1991 *Int. J. Mod. Phys.* **2** 371
[18] Mikhailovskii A B, Huysmans G T A, Kerner W O K and Sharapov S E 1997 *Plasma Phys. Rep.* **23** 844
[19] Borba D and Kerner W 1999 *J. Comput. Phys.* **153** 101 – 138

[20] Nabais F, Borba D, Coelho R, Figueiredo A, Ferreira J, Loureiro N and Rodrigues P 2015 *Plasma Sci. Technol.* **17** 89
[21] Pereverzev G and Corrigan G 2008 *Comp. Phys. Comm.* **179** 579–585
[22] Hole M J, von Nessi G, Fitzgerald M and the MAST team 2013 *Plasma Phys. Control. Fusion* **55** 014007